Multimed Tools Appl (2015) 74:1983–1995
DOI 10.1007/s11042-013-1733-0

An adaptive reversible steganographic scheme based on the just noticeable distortion

Chuan Qin · Chin-Chen Chang · Chia-Chun Lin

Published online: 10 October 2013

Abstract In this paper, we propose an adaptive reversible steganographic scheme based on the just noticeable distortion (JND). First, the JND value of each cover pixel is calculated using the frequency model of the human visual system (HVS). Then, the prediction value of the cover pixel is acquired by anisotropic interpolation, and also the pixel distribution characteristic is estimated. Finally, whether the cover pixel is embeddable or not is adaptively determined according to the relationship between the prediction error and the JND value. The embedding procedure is based on modifying the prediction error of each cover pixel, and the visual degradation caused by embedding is imperceptible due to the control of JND. Experimental results demonstrate that the proposed scheme provides a greater embedding rate and higher quality of stego image than other methods that have been reported recently.

Keywords Reversible data hiding · Just noticeable distortion · Embedding rate · Visual quality

1 Introduction

Steganography, also called data hiding, is a technique that embeds data into a cover medium in an irreversible or reversible manner, which can be used for covert communication and

C. Qin
School of Optical-Electrical and Computer Engineering, University of Shanghai for Science and Technology, Shanghai 200093, China
e-mail: qin@usst.edu.cn

C.-C. Chang (✉)
Department of Information Engineering and Computer Science, Feng Chia University, 100 Wenhwa Road, Taichung 40724, Taiwan
e-mail: alan3c@gmail.com

C.-C. Chang
Department of Computer Science and Information Engineering, Asia University, Taichung 41354, Taiwan

C.-C. Lin
Department of Computer Science and Information Engineering, National Chung Cheng University, Chiayi 62102, Taiwan
e-mail: leonn1046@gmail.com

copyright protection etc. For some important cover medium, such as medical and military images, the property of reversibility of data hiding is essential, which means that the original form of the image, before the secret data were embedded, must be completely recoverable after the embedded data are extracted. In addition to hiding capacity, the quality of the stego image is also a key point of the researches on reversible data hiding because, the higher the quality of stego image is, the less likely it becomes that an adversary could identify the presence of hidden information [1, 3, 4, 9, 12].

Recently, a large number of reversible data hiding schemes have been developed for cover images in various forms, such as color images [4], gray-level images [12], and compressed images [1]. Difference expansion and histogram shifting are the two most common techniques used in reported reversible data hiding schemes. In the difference expansion based schemes, such as [12], the differences of the non-overlapping, neighboring pixel pairs in the cover image were doubled and then modified according to the parity of the embedding secret bits. In the histogram-shifting based schemes, such as [9], the peak point of the cover image histogram was chosen, and the pixel values in the range from its right one to the zero point were increased by one to create one vacant histogram bin for secret data embedding. In the schemes of [5–8, 10, 11, 13, 16], the prediction mechanism was integrated. These kinds of prediction-based schemes first conducted the prediction process to estimate the cover image pixels, and the prediction error, i.e., the difference between the cover pixel and the prediction result, was used to embed the secret data by difference expansion [7, 8] or histogram shifting [5, 6, 10, 11, 13, 16]. The consistency of the prediction results in the embedding and extracting procedures ensures the correctness of the extraction of the secret bits and the recovery of the cover image.

Usually, the higher the hiding capacity is in reversible data hiding schemes, the lower the visual quality of stego image becomes. Although the operations of difference expansion and histogram shifting can create some spare space for data embedding, severe distortions occur between the stego image and the cover image. However, unsatisfactory visual quality of the stego image may not be acceptable in data hiding, especially for covert communication, because images that are obviously degraded must attract the attention of adversaries who may use steganalysis tools to conduct an attack. Therefore, it is important to consider the characteristics of the image content and human visual sensitivity when embedding data to reduce the degradation of the stego image as much as possible.

In this paper, we propose an adaptive reversible steganographic scheme based on the human visual system (HVS). By taking advantage of the sensitivities of the frequency components, the value of the just noticeable distortion (JND) for each cover image pixel is calculated. Then, the anisotropic interpolation is adopted to conduct pixel prediction and produce smaller prediction errors. The distribution characteristic of cover image pixel and the relationship between the JND value and the prediction error are analyzed to adaptively decide whether the current pixel is suitable for secret bit embedding or not. Due to the adjustment by the JND values, the complex regions and the regions with smaller prediction errors can be embedded with more secret bits, which can simultaneously reduce the visual distortion and provide satisfactory hiding capacity.

The rest of the paper is organized as follows. Section 2 reviews the typical reported reversible data hiding schemes. Section 3 describes the detailed procedures of the proposed scheme based on the JND mechanism. Experimental results and comparisons are presented in Section 4, and conclusions are finally drawn in Section 5.

2 Related works

Earlier research on reversible data hiding by Fridrich et al. focused on compressing the chosen subset of original cover image, such as lower bit-planes, losslessly and replacing the chosen bit-planes with the concatenated bits of its compressed version and the secret bits for hiding [3]. The hiding capacity of this kind of method depended on the difference of data amounts of the chosen bit-planes before and after lossless compression. Higher payloads forced more bit-planes to be used, which may quickly increase perceptible distortions on cover image beyond an acceptable level. Fridrich et al. improved their prior method by defining a discrimination function and an invertible flipping operation in [4]. According to the discrimination function, all disjoint pixel groups in cover image were categorized into three types, i.e., regular groups, singular groups, and unusable groups. The regular groups and the singular groups corresponded to the binary bits, i.e., 1 and 0, respectively, and the unusable groups can not be used for embedding. If the secret bit and the group type didn't match, the flipping operation was applied to the group to obtain a match. Thus, each regular and singular group can be embedded with one bit. However, in order to achieve the reversibility, the vector indicating the original status of regular and singular groups should be losslessly compressed and then be embedded as extra information bits together with secret bits. Because only parts of the pixel groups can be used and the extra information bits occupied some embedding space, the hiding capacity of this method was not high enough.

In the recent years, the techniques of difference expansion and histogram shifting were introduced into reversible data hiding. Tian first proposed a reversible data hiding scheme using the difference expansion technique [12]. In his work, the cover image was divided into a series of non-overlapping, neighboring pixel pairs, and the differences of the pixel pair that were smaller than a pre-determined threshold were doubled. Then, the doubled differences were either kept reserved or modified to match the parity of the secret bits for embedding. The receiver can easily extract the embedded secret bits from the least significant bits (LSB) of the differences of the pixel pairs in stego image. However, the doubled differences of pixel pairs severely degraded the stego image quality, and the extra information for solving the underflow and overflow problems should also be embedded, which decreased the pure capacity of this method. A histogram shifting based method was proposed by Ni et al. in [9]. The pixel values in the range from the right one of the histogram peak point to the nearest zero point were all increased by one to create one vacant histogram bin for embedding. The pixel values corresponding to the peak point were utilized for data embedding, which were either kept intact or modified by one level according to the secret bits. But, for some cover images with flat distribution of histograms, the hiding capacity of this method was not satisfactory. Additionally, the information of peak point and zero point should also be transmitted to the receiver side for data extraction and image recovery.

In order to further improve the performances of hiding capacity and stego image quality, the prediction mechanism has been utilized in recent studies. Instead of directly using the original image, the prediction based schemes used the prediction errors as the cover data for embedding [5–8, 10, 11, 13, 16]. Lee et al. proposed a prediction based method using difference expansion [7]. Because most of the differences between the cover pixels and the corresponding prediction values are small, the large quantities of prediction errors can be used to embed secret bits by exploiting the

expansion, which can achieve greater hiding capacity than [12]. Hong et al. tried the bi-linear interpolation and the bi-cubic interpolation to predict the cover image according to the selected reference pixels [5]. Then, the histogram of prediction errors was shifted to embed the secret bits. Based on the above analysis, we can find that the prediction technique and the embedding strategy of prediction errors are the two key points of the prediction based reversible data hiding schemes. In the subsequent section, a novel scheme using the anisotropic interpolation based prediction and the HVS sensitivity based embedding strategy is presented.

3 Proposed scheme

In the proposed scheme, the data embedding procedure is conducted on cover image pixels in raster-scanning order, and JND value, prediction error and the distribution characteristic of the current processing pixel depend totally on its previous processed pixels. Consequently, during the extraction and recovery procedure, the recovered pixels can assist the secret data extraction and pixel recovery for the subsequent pixels in raster-scanning order.

Before embedding, a pre-processing step should be implemented on the cover image to avoid the overflow and underflow problems caused by embedding. A threshold, i.e., λ, is set to ensure that the gray values of all pixels after embedding are changed no more than 2^{λ}. All cover pixels valued at $[0, 2^{\lambda} - 1]$ and $[255 - 2^{\lambda} + 1, 255]$ are modified to 2^{λ} and $255 - 2^{\lambda}$, respectively. To achieve reversibility, the auxiliary information that records the modifications of this pre-processing step is compressed by a run-length coder and appended with the pure secret data to generate the final to-be-embedded bits. Thus, the procedures of JND calculation and data embedding are applied on the pre-processed cover image rather than the original cover image.

3.1 JND calculation

Various HVS models have been proposed to describe the sensitivity of human eyes for images, and the JND value of an HVS model denotes the smallest change in a pixel value that the human eyes can perceive. Basically, the HVS model can be constructed either in spatial domain [2] or frequency domain [15]. In this work, we utilize an HVS model derived from the frequency domain of discrete cosine transform (DCT) [15]. This model treats each DCT coefficient as an approximation to the local response of a visual channel, and an 8×8 perceptual error matrix, i.e., the Watson matrix, is generated for the DCT coefficients of each image block by the adjustment of contrast sensitivity, light adaptation, and contrast masking. Two perceptual modes are provided in this HVS model, i.e., image-independent perceptual (IIP) mode and image-dependent perceptual (IDP) mode. In this work, the IIP mode is used for JND calculation.

The cover image $\mathbf{I}$ sized $M \times N$ is first divided into $M / 8$ parts with the same size horizontally, i.e., $\mathbf{H}_1, \mathbf{H}_2, \ldots, \mathbf{H}_{M/8}$, and the first eight columns of $\mathbf{I}$ are kept unchanged and embedded with no secret data. Thus, for each $\mathbf{H}_i$ (i=1, 2, …, $M / 8$), there are $8N-64$ cover pixels that can be used for data embedding. Denote the first $N-8$ overlapping blocks sized 8×8 in $\mathbf{H}_i$ as $\mathbf{B}_k^{(i)}$ (k=1, 2, …, $N-8$), and each $\mathbf{B}_k^{(i)}$ consists of the pixels $I(x, y)$, where $x=8i-7, 8i-6, \ldots, 8i$, and $y=k, k+1, \ldots, k+7$. We conduct DCT transform on each $\mathbf{B}_k^{(i)}$, and the obtained DCT coefficient matrix is expressed as $\mathbf{C}_k^{(i)}$. The Watson matrix $\mathbf{\Psi}$, which denotes

the largest tolerable variation of each DCT coefficient for imperceptibility by human eyes, is shown in Eq. (1).

$$\mathbf{\Psi} = \begin{pmatrix} 1.40 & 1.01 & 1.16 & 1.66 & 2.40 & 3.43 & 4.79 & 6.56 \\ 1.01 & 1.45 & 1.32 & 1.52 & 2.00 & 2.71 & 3.67 & 4.93 \\ 1.16 & 1.32 & 2.24 & 2.59 & 2.98 & 3.64 & 4.60 & 5.88 \\ 1.66 & 1.52 & 2.59 & 3.77 & 4.55 & 5.30 & 6.28 & 7.60 \\ 2.40 & 2.20 & 2.98 & 4.55 & 6.15 & 7.46 & 8.71 & 10.17 \\ 3.43 & 2.71 & 3.64 & 5.30 & 7.46 & 9.62 & 11.58 & 13.51 \\ 4.79 & 3.67 & 4.60 & 6.28 & 8.71 & 11.58 & 14.50 & 17.29 \\ 6.56 & 4.93 & 5.88 & 7.60 & 10.17 & 13.51 & 17.29 & 21.15 \end{pmatrix}. \tag{1}$$

The JND values for each $\mathbf{B}_k^{(i)}$ can be calculated using Eqs. (2)–(4):

$$\widehat{\mathrm{C}}_k^{(i)}(x,y) = \left[\left|\mathrm{C}_k^{(i)}(x,y)\right| + \Psi(x,y)\right]\cdot\mathrm{sign}\left[\mathrm{C}_k^{(i)}(x,y)\right], \tag{2}$$

$$\widehat{\mathbf{B}}_k^{(i)} = \mathrm{IDCT}\left(\widehat{\mathbf{C}}_k^{(i)}\right), \tag{3}$$

$$\mathrm{JND}_k^{(i)}(x,y) = \left|\widehat{\mathrm{B}}_k^{(i)}(x,y) - \mathrm{B}_k^{(i)}(x,y)\right|, \tag{4}$$

where IDCT denotes the inverse discrete cosine transform, the function sign(·) returns the sign of the input parameter, and $\mathrm{JND}_k^{(i)}(x,y)$ is the JND value for each pixel $\mathrm{B}_k^{(i)}(x,y)$ in block $\mathbf{B}_k^{(i)}$. As stated at the beginning of Section 3, the JND value of the current pixel should be derived from its previous pixels in raster-scanning order for reversibility. Thus, the JND values of all the $M(N-8)$ cover pixels that can be used for data embedding in $\mathbf{H}_i$ (i=1, 2, …, M / 8) are estimated using the JND values of their left pixels directly, i.e., JND(x, y) ← JND(x, y−1), where x=1, 2, …, M and y=9, 10, …, N. The estimated JND values are then adjusted by the nonlinear function in Eq. (5) to make it more suitable for data embedding.

$$\mathrm{JND}^*(x,y) = e^{\mathrm{JND}(x,y)}\cdot 2^{\lambda-1}. \tag{5}$$

3.2 Data embedding

The embedding procedure of the proposed scheme is based on the expansion of prediction error. Thus, before embedding, the prediction value of each embeddable pixel should be computed. We denote the neighboring region of the current pixel $I(x, y)$ for embedding as $\Omega_{x,y}$, and all K pixels in $\Omega_{x,y}$ are at the previous of $I(x, y)$ in raster-scanning order. The prediction value for $I(x, y)$ is obtained by Eq. (6):

$$I_p(x,y) = \sum_{i=1}^{K} \alpha_i \cdot I(x_i,y_i), \quad \forall\ (x_i,y_i) \in \Omega_{x,y}, \tag{6}$$

where α_i is the weight of each pixel in $\Omega_{x,y}$ for contributing to the prediction value, and $\sum\alpha_i \equiv 1$ for all i=1, 2,…, K. Essentially, Eq. (6) is an anisotropic interpolation model. In our

scheme, α_i is inversely proportional to the distance between $I(x_i, y_i)$ and $I(x, y)$. The prediction error of each embeddable pixel is defined as: $\sigma(x, y) = I(x, y) - I_p(x, y)$.

Inspired by the scheme in [6], in order to apply the different embedding conditions for the regions with different distributions, we estimate the distribution characteristic of each possible embeddable pixel to judge whether it is located in smooth region or complex region. If the variance of the neighboring region $\Omega_{x,\,y}$ of the current pixel $I(x, y)$ is smaller than a pre-determined threshold T, $I(x, y)$ is judged as a smooth pixel. Otherwise, $I(x, y)$ is judged as a complex pixel. For each smooth pixel $I(x, y)$, the embedding level $L_{x,\,y}$ is calculated by:

$$L_{x,y} = \min\left\{\left\lfloor \log_2\left[\mathrm{JND}^*(x,y)\right]\right\rfloor, \lambda\right\}. \tag{7}$$

For each complex pixel $I(x, y)$, the embedding level $L_{x,\,y}$ is calculated by:

$$L_{x,y} = \min\left\{\left\lceil \log_2\left[\mathrm{JND}^*(x,y)\right]\right\rceil, \lambda\right\}, \tag{8}$$

where $\lfloor\cdot\rfloor$ and $\lceil\cdot\rceil$ denote the nearest integers no greater than and no smaller than the input, respectively, and these two functions imply that the complex region can tolerate more embedding distortions than the smooth region due to the relative insensitivity of the human eyes.

In order to alleviate degradation, the embedding of secret data is conducted only on the pixels $I(x, y)$, whose absolute values of prediction errors $\sigma(x, y)$ are smaller than $2^{L_{x,\,y}}$, see Eq. (9).

$$I_s(x,y) = \begin{cases} I(x,y) + \sigma(x,y) + \mathrm{sign}[\sigma(x,y)]\cdot s, & \text{if } |\sigma(x,y)| < 2^{L_{x,y}}, \\ I(x,y) + \mathrm{sign}[\sigma(x,y)] \cdot 2^{L_{x,y}}, & \text{if } |\sigma(x,y)| \geq 2^{L_{x,y}}, \end{cases} \tag{9}$$

where $s \in \{0, 1\}$ is the current secret bit to be embedded, and $I_s(x, y)$ is the stego pixel. After all the secret bits and the auxiliary information have been embedded, the embedding procedure is finished, and the resulting stego image I_s can be transmitted to the receiver side.

3.3 Data extraction and image recovery

To guarantee successful extraction and recovery, the parameters λ and T must be shared by the receiver side. The procedure of data extraction and image recovery is also conducted on the stego image progressively in raster-scanning order, except for the unchanged $8M$ pixels in the first eight columns. Thus, the same results of JND value, prediction value, and embedding level for the stego pixels can be acquired.

Denote the current stego pixel as $I_s(x, y)$. As stated above, the prediction value of $I_s(x, y)$ is still $I_p(x, y)$. The prediction error of the stego pixel is defined as: $\sigma_s(x, y) = I_s(x, y) - I_p(x, y)$. If $|\sigma_s(x, y)| < 2^{L_{x,\,y}+1}$, it means that the current stego pixel $I_s(x, y)$ is embedded with one secret bit. Otherwise, the current pixel is only modified without having any secret bit embedded. Therefore, secret bit extraction and image recovery can be achieved by Eqs. (10) and (11), respectively.

$$s = \mathrm{mod}(|\sigma_s(x,y)|, 2), \quad \text{subject to } |\sigma_s(x,y)| < 2^{L_{x,y}+1}, \tag{10}$$

$$I(x,y) = \begin{cases} I_s(x,y) - \mathrm{sign}[\sigma_s(x,y)]\cdot\left\lceil \dfrac{|\sigma_s(x,y)|}{2} \right\rceil, & \text{if } |\sigma_s(x,y)| < 2^{L_{x,y}+1}, \\ I_s(x,y) - \mathrm{sign}[\sigma_s(x,y)] \cdot 2^{L_{x,y}}, & \text{if } |\sigma_s(x,y)| \geq 2^{L_{x,y}+1}, \end{cases} \tag{11}$$

where s is the extracted secret bit from the current stego pixel $I_s(x, y)$, and $I(x, y)$ is the recovered pixel value. After all embedded secret bits have been extracted, the auxiliary information bits can be retrieved to further recover the pixels modified in the pre-processing step, and then, the original image can be acquired successfully.

Different with the reported reversible steganographic schemes, the proposed scheme adopts the anisotropic interpolation in the prediction process of cover pixels, which can obtain better prediction accuracy and smaller prediction errors than traditional prediction technique based on the isotropic interpolation. Furthermore, the proposed scheme doesn't utilize the fixed embedding level to decide whether the cover pixels are embeddable or not. In order to achieve satisfactory performances of the hiding capacity and the stego image quality simultaneously, the embedding level of each cover pixel is adaptively calculated according to its JND value and distribution characteristic. In our scheme, the JND value of each pixel derives from the frequency domain based HVS model, which can be used to guarantee the visual quality of stego image acceptable. Each cover pixel is also classified into smooth pixel or complex pixel by its distribution characteristic based on the neighborhood variance. Since complex region can tolerate more distortions than smooth region, we adjust the embedding levels of complex pixels higher than those of smooth pixels to embed more bits without causing severe distortions. By these strategies, compared with the reported schemes, the proposed scheme can achieve greater hiding capacity under the similar quality of stego image.

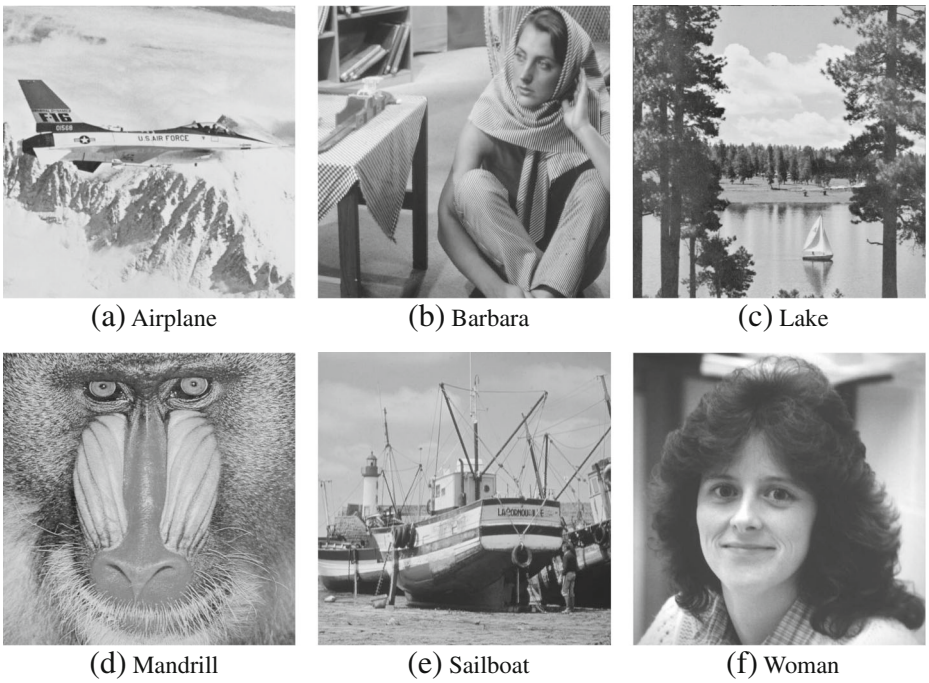

(a) Airplane (b) Barbara (c) Lake

(d) Mandrill (e) Sailboat (f) Woman

Fig. 1 Six standard test images

4 Experimental results and comparisons

Experiments were conducted on a group of gray-level images to evaluate hiding capacity and visual quality of stego image of the proposed scheme. We used the embedding rate R to represent the pure hiding capacity, as shown in Eq. (12).

$$R = \frac{L - L_a}{M \times N}(\text{bpp}), \tag{12}$$

where L is the number of all embedded bits, L_a is the number of the compressed auxiliary information bits within all embedded bits, and bpp denotes bits per pixel. Two typical measurement indices, i.e., peak signal-to-noise ratio (PSNR) and structural similarity (SSIM), were used to assess the visual quality of the stego image. The measure of SSIM was developed based on the characteristics of the HVS, which integrated the information of structure, luminance and contrast synthetically for the image quality assessment [14].

The six standard, 512×512 images that were used for testing, i.e., *Airplane*, *Barbara*, *Lake*, *Mandrill*, *Sailboat*, and *Woman*, are shown in Fig. 1. The threshold T used for the estimation of pixel distribution was set as 200 in the experiments. Figure 2 shows six stego versions of the images in Fig. 1, and the embedding rates R are 0.8249 bpp, 0.6229 bpp, 0.6430 bpp, 0.4123 bpp, 0.7382 bpp, and 0.9134 bpp, respectively. We can observe from Fig. 2 that the stego images have good visual quality and that the distortions caused by embedding are imperceptible to the human eyes.

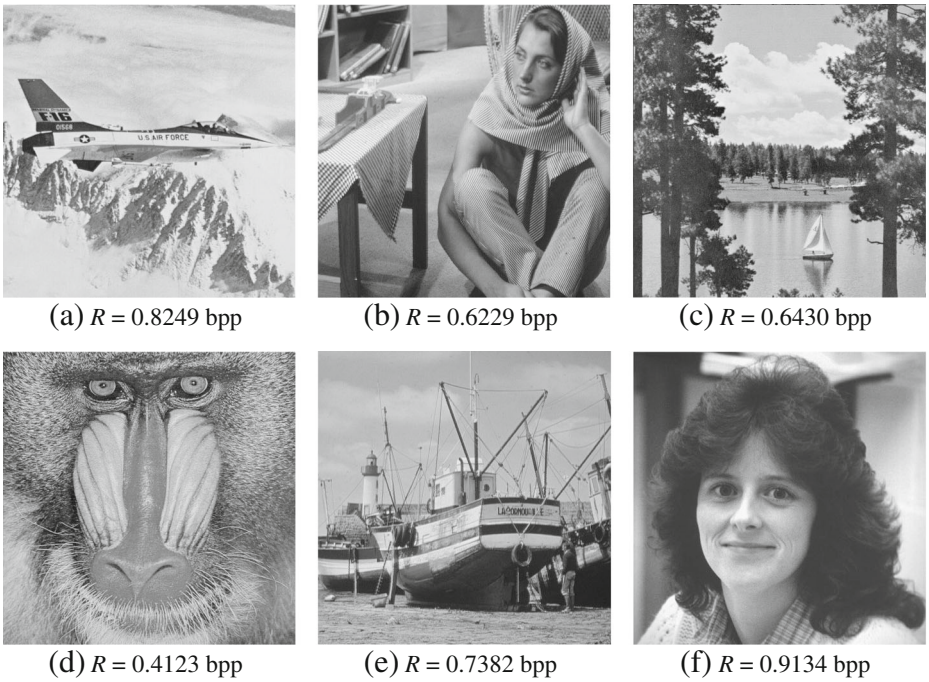

(a) R = 0.8249 bpp (b) R = 0.6229 bpp (c) R = 0.6430 bpp

(d) R = 0.4123 bpp (e) R = 0.7382 bpp (f) R = 0.9134 bpp

Fig. 2 Stego images of the six test images in Fig. 1 (λ=3). **a** PSNR=36.0689 dB, SSIM=0.9832; **b** PSNR=33.4088 dB, SSIM=0.9820; **c** PSNR=33.3851 dB, SSIM=0.9842; **d** PSNR=31.9036 dB, SSIM=0.9807; **e** PSNR=34.5814 dB, SSIM=0.9824; **f** PSNR=37.6211 dB, SSIM=0.9844

Table 1 Performances of the proposed scheme with different thresholds λ

Images		λ=0	λ=1	λ=2	λ=3	λ=4
Airplane	*R*	0.1775	0.4091	0.6636	0.8249	0.9152
	PSNR	48.6096	43.8340	39.6167	36.0689	32.9304
	SSIM	0.9982	0.9951	0.9895	0.9832	0.9762
Barbara	*R*	0.0782	0.2046	0.4161	0.6229	0.7738
	PSNR	48.3753	43.0546	37.9367	33.4088	29.2682
	SSIM	0.9991	0.9970	0.9918	0.9820	0.9663
Lake	*R*	0.0690	0.1836	0.3831	0.6430	0.8542
	PSNR	48.3542	43.0218	37.8172	33.3851	30.0944
	SSIM	0.9992	0.9975	0.9930	0.9842	0.9721
Mandrill	*R*	0.0342	0.0940	0.2153	0.4123	0.6464
	PSNR	48.2760	42.6911	37.0819	31.9036	27.4043
	SSIM	0.9994	0.9979	0.9930	0.9807	0.9586
Sailboat	*R*	0.1056	0.2758	0.5306	0.7382	0.8802
	PSNR	48.4386	43.3187	38.5776	34.5814	31.2226
	SSIM	0.9988	0.9965	0.9914	0.9824	0.9696
Woman	*R*	0.2104	0.4819	0.7491	0.9134	0.9727
	PSNR	48.6900	44.1158	40.3303	37.6211	35.2421
	SSIM	0.9981	0.9949	0.9897	0.9844	0.9766

It can be found from Eqs. (7)–(9) that the parameter λ is closely related to the hiding capacity and the degradation of visual quality. Table 1 presents the performances of the proposed scheme with respect to embedding rate *R* and visual quality after embedding with different λ. We can find that the embedding rate *R* becomes greater with the increase of λ, but the visual quality of the stego images becomes worse. We also evaluated the relationship between the embedding rate *R* and the threshold *T* used for the estimation of pixel distribution. As described in Subsection 3.2, if the variance of the neighboring region of the current pixel $I(x, y)$ is smaller than the threshold *T*, $I(x, y)$ is judged as a smooth pixel. Otherwise, $I(x, y)$ is judged as a complex pixel. Obviously, smaller threshold *T* causes that more pixels are judged as the complex pixels. Equations (7) and (8) correspond to the

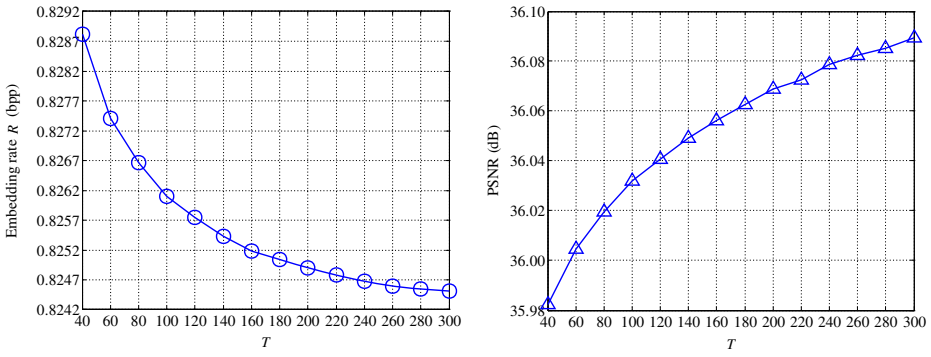

Fig. 3 The relationships between the embedding rate *R* and PSNR value with the threshold *T*

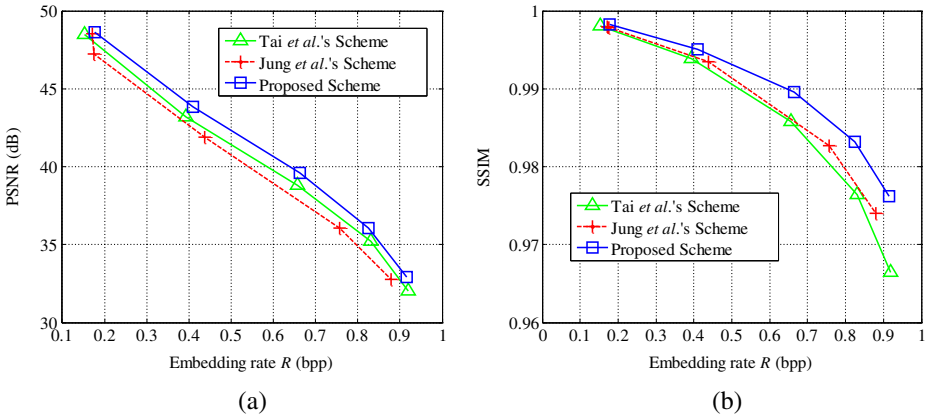

(a) (b)

Fig. 4 Performance comparisons of the proposed scheme and the schemes in [6, 11] for *Airplane*. **a** Embedding rate R versus PSNR, **b** embedding rate R versus SSIM

calculation of embedding level for the smooth pixel and the complex pixel, respectively. We can clearly find that, for a given pixel $I(x, y)$, the embedding level $L_{x,y}$ calculated by Eq. (8) is always not smaller than that calculated by Eq. (7), and according to Eq. (9), larger embedding levels make more pixels embeddable. Therefore, smaller threshold T leads to greater embedding rate and lower PSNR value consequently. Figure 3(a) and (b) show the curves of the relationships between the embedding rate R and PSNR value with the threshold T for *Airplane* (λ=3), respectively, which is consistent with the result of above analysis.

We compared our scheme with two typical schemes that were reported recently, i.e., Tai et al.'s scheme [11] and Jung et al.'s scheme [6]. Figures 4, 5 and 6 show the comparison results for the three schemes, and (a) and (b) in these figures are the corresponding results of embedding rate versus PSNR and SSIM, respectively. Note that the neighboring region for the calculations of prediction value and embedding level in our scheme was selected in the same way as the causal window in [6], and the size is 3. As shown in Figs. 4, 5 and 6, for the same embedding rate, Jung et al.'s scheme [6], which also considered the human visual system, outperforms Tai et al.'s scheme [11] with respect to SSIM; however, it is not obviously superior

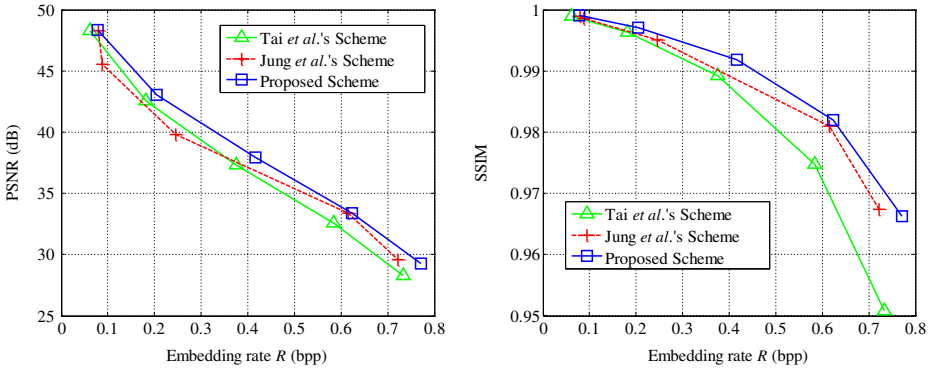

(a) (b)

Fig. 5 Performance comparisons of the proposed scheme and the schemes in [6, 11] for *Barbara*. **a** Embedding rate R versus PSNR, **b** embedding rate R versus SSIM

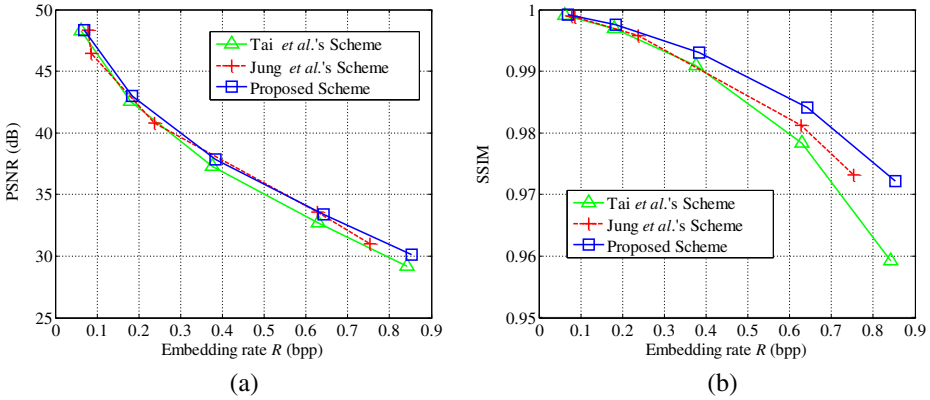

Fig. 6 Performance comparisons of the proposed scheme and the schemes in [6, 11] for *Lake*. **a** Embedding rate R versus PSNR, **b** embedding rate R versus SSIM

to Tai et al.'s scheme with respect to PSNR. Due to the appropriate control by the JND values, we can find from the comparison results that the proposed scheme has better performances of both PSNR and SSIM versus embedding rate than the schemes in [6, 11].

5 Conclusions

In this work, an adaptive reversible steganographic scheme for high-quality images based on HVS is proposed. The JND value of each embeddable cover pixel is calculated by using the Watson matrix of the IIP model in the DCT frequency domain. By analyzing the characteristics of pixel distribution, the embedding strategy utilizes the relationship between JND values and prediction errors to adaptively decide whether cover pixels can be embedded with secret bits or not. Because the modification of each pixel caused by embedding is controlled by its JND value and the pre-determined threshold, the degradation of visual quality is imperceptible to the human eyes. Compared with other schemes that have been reported recently, the proposed scheme has a greater embedding rate and higher visual quality of the stego image. A future improvement that can be made is to integrate the IDP model into the current scheme for better performance.

Acknowledgments This work was supported by the Natural Science Foundation of China (61303203), the Natural Science Foundation of Shanghai, China (13ZR1428400), the Innovation Program of Shanghai Municipal Education Commission (14YZ087), and the OECE Innovation Foundation of USST.

References

1. Chang CC, Lin CC, Tseng CS, Tai WL (2007) Reversible hiding in DCT-based compressed images. Inf Sci 177(13):2768–2786
2. Chou CH, Li YC (1995) A perceptually tuned subband image coder based on the measurement of just-noticeable-distortion profile. IEEE Trans Circ Syst Video Technol 5(6):467–476
3. Fridrich J, Goljan M, Du R (2001) Invertible authentication. Proceedings of SPIE Security and Watermarking of Multimedia Contents III, San Jose, vol. 4314, pp 197–208
4. Fridrich J, Goljan M, Du R (2002) Lossless data embedding—new paradigm in digital watermarking. EURASIP J Appl Signal Process 2002(2):185–196

5. Hong W, Chen TS (2011) Reversible data embedding for high quality images using interpolation and reference pixel distribution mechanism. J Vis Commun Image Represent 22(2):131–140
6. Jung SW, Ha LT, Ko SJ (2011) A new histogram modification based reversible data hiding algorithm considering the human visual system. IEEE Signal Process Lett 18(2):95–98
7. Lee CF, Chen HL, Tso HK (2010) Embedding capacity raising in reversible data hiding based on prediction of difference expansion. J Syst Softw 83(10):1864–1872
8. Liu YC, Wu HC, Yu SS (2011) Adaptive DE-based reversible steganographic technique using bilinear interpolation and simplified location map. Multimed Tools Appl 52(2–3):263–276
9. Ni ZC, Shi YQ, Ansari N, Su W (2006) Reversible data hiding. IEEE Trans Circ Syst Video Technol 16(3):354–362
10. Qin C, Chang CC, Huang YH, Liao LT (2013) An inpainting-assisted reversible steganographic scheme using a histogram shifting mechanism. IEEE Trans Circ Syst Video Technol 23(7):1109–1118
11. Tai WL, Yeh CM, Chang CC (2009) Reversible data hiding based on histogram modification of pixel differences. IEEE Trans Circ Syst Video Technol 19(6):906–910
12. Tian J (2003) Reversible data embedding using a difference expansion. IEEE Trans Circ Syst Video Technol 13(8):890–896
13. Tsai P, Hu YC, Yeh HL (2009) Reversible image hiding scheme using predictive coding and histogram shifting. Signal Process 89(6):1129–1143
14. Wang Z, Bovik AC, Sheikh HR, Simoncelli EP (2004) Image quality assessment: from error visibility to structural similarity. IEEE Trans Image Process 13(4):600–612
15. Watson AB (1993) DCT quantization matrices visually optimized for individual images. Proceedings of SPIE Human Vision, Visual Processing, and Digital Display IV, Bellingham, WA, pp 202–216
16. Zhao Z, Luo H, Lu ZM, Pan JS (2011) Reversible data hiding based on multilevel histogram modification and sequential recovery. Int J Electron Commun 65(10):814–826

Chuan Qin received the B.S. and M.S. degrees in electronic engineering from Hefei University of Technology, Anhui, China, in 2002 and 2005, respectively, and the Ph.D. degree in signal and information processing from Shanghai University, Shanghai, China, in 2008. Since 2008, he has been with the faculty of the School of Optical-Electrical and Computer Engineering, University of Shanghai for Science and Technology, where he is currently a Lecturer. He also has been with Feng Chia University at Taiwan as a Postdoctoral Researcher from July 2010 to June 2012. His research interests include image processing and multimedia security.

Chin-Chen Chang received his B.S. degree in applied mathematics in 1977 and the M.S. degree in computer and decision sciences in 1979, both from the National Tsing Hua University, Hsinchu, Taiwan. He received his Ph.D in computer engineering in 1982 from the National Chiao Tung University, Hsinchu, Taiwan. During the academic years of 1980–1983, he was on the faculty of the Department of Computer Engineering at the National Chiao Tung University. From 1983 to 1989, he was on the faculty of the Institute of Applied Mathematics, National Chung Hsing University, Taichung, Taiwan. From August 1989 to July 1992, he was the head of, and a professor in, the Institute of Computer Science and Information Engineering at the National Chung Cheng University, Chiayi, Taiwan. From August 1992 to July 1995, he was the dean of the college of Engineering at the same university. From August 1995 to October 1997, he was the provost at the National Chung Cheng University. From September 1996 to October 1997, Dr. Chang was the Acting President at the National Chung Cheng University. From July 1998 to June 2000, he was the director of Advisory Office of the Ministry of Education of Taiwan. From 2002 to 2005, he was a Chair Professor of National Chung Cheng University. Since February 2005, he has been a Chair Professor of Feng Chia University. In addition, he has served as a consultant to several research institutes and government departments. His current research interests include database design, data structures, computer cryptography and image processing. He is a fellow of the IEEE.

Chia-Chun Lin received the B.S. degree in applied mathematics from Feng Chia University, Taiwan. He is currently pursuing the M.S. degree in computer science and engineering from National Chung Cheng University. His research interests include data hiding and secret sharing.